A relationship of porosity and mechanical properties of spark plasma sintered scandia stabilized zirconia thermal barrier coating

AKM Asif Iqbal [a,*], Mei Jing Lim [b]

[a] Department of Mechanical, Materials and Manufacturing Engineering, Faculty of Science and Engineering, University of Nottingham Ningbo China, 199 Taikang East Road, Ningbo, 315100, China
[b] Faculty of Manufacturing and Mechatronic Engineering Technology, University Malaysia Pahang (UMP), 26600, Pekan, Pahang, Malaysia

ABSTRACT

Porous ceramic materials are popularly accepted as thermal barrier coatings (TBCs) in insulating gas turbine parts working at high temperatures. In this research, three different types of Scandia stabilized zirconia (ScSZ) systems, a nanometric 10 mol% ScSZ (10-ScSZ), a micrometric 8 mol% ScSZ (8-ScSZ) and a combination of these two powders (10-8-ScSZ) have been developed by Spark Plasma Sintering (SPS) process. Varying SPS parameters, for instance, temperature, pressure and dwell time were applied to develop the different volumes of porosity in the materials. Subsequently, the microstructure of the materials has been studied and mechanical properties have been evaluated. All three materials demonstrate a reduced porosity level at high sintering temperature and pressure. However, the nanometric 10-ScSZ material shows a higher reduction of porosity from 51.8% to 11.1% at 30 MPa pressure and 40.2%–8.5% at 60 MPa pressure within the temperature range of 1000–1200 °C. Besides, the 10-8-ScSZ composite exhibits substantially increased porosity in comparison to its constituent parts. The results also show that the nanometric 10-ScSZ material exhibits a greater mechanical strength including Vickers microhardness of 81 HV, flexural strength of 361 MPa and elastic modulus of 187 GPa at 5% porosity level, as compared to the other two materials. Additionally, it is observed that all the mechanical properties for all three materials consistently decrease with the increase in porosity levels. While compared with the traditional atmospheric plasma spray (APS) processed ceramic coating, the porous ScSZ coating materials exhibit a larger elastic modulus. Therefore, the porous ScSZ developed by the SPS process could be a prospective alternative thermal barrier coating (TBC).

1. Introduction

Thermal barrier coatings (TBCs) are extensively used as an insulator for the components working at high temperatures in the gas turbine engine. The TBCs are deposited on the metallic parts to protect them against oxidation and corrosion and eventually enhance the durability of the gas turbine [1,2]. The ideal properties of a thermal barrier coating system include low thermal conductivity, phase stability under prolonged high-temperature exposure, high thermal cycling resistance, thermal expansion matching with the metallic substrate, chemical inertness, good adhesion to the metallic substrate, and a low sintering rate of the porous microstructure [2]. Generally, a conventional TBC is a double-layered coating containing a ceramic topcoat and a metallic bond coat [3]. TBCs are often produced by using the atmospheric plasma spray (APS) process. The thermal conductivity of the TBCs created using

the APS approach is approximately 0.812 W/mK [4]. According to the previous work, a certain level of the porousness of the material shows a positive impact on reducing the thermal transformation of TBCs. It has been noted that an increase in porosity level of more than 30 vol% reduces the thermal conductivity as low as 0.4 W/mK [5]. However, the mechanical properties of this kind of ceramics need to be evaluated properly before exposing them to the harsh environment [6].

There have been several attempts to create porous ceramics, and as a result, numerous techniques have been used. These procedures include partial sintering of powdered materials, direct foaming, slip casting, gel casting, tape casting and the template approach [7–12]. However, producing porous ceramic using non-conventional techniques like Spark plasma sintering (SPS) has been scarcely reported. The SPS technique has gained recognition as a successful technology because it can create materials with controlled microstructure and structured phase

composition [13–15]. SPS employs electric current and pressure to produce high-performance ceramic materials while preserving a fine-grained structure [16–18]. Numerous studies have discussed the great mechanical strength that SPS-produced nanoceramics have attained. These results demonstrated that nanoparticles may maintain their position in the presence of significant densification because of the robust sintering kinetics of the SPS method [19–22]. Chevalier et al. [23] discussed the behaviour of mechanical properties of SPS sintered Yttria Stabilized Zirconia (YSZ) and concluded that due to the impressive mechanical properties, this material is now being popularly introduced in many applications including thermal barriers. In addition, Monceau et al. [24] produced a superalloy substrate using a one-step sintering process utilizing SPS and then coated a porous ceramic layer on it. They discovered the prepared TBCs to have excellent strength and durability even after 1000 cycles at 1100 °C. On the other hand, Spriggs et al. [25] developed YSZ ceramic via partial sintering but noted that this material had average mechanical characteristics. Due to its high thermal resistivity and a high coefficient of thermal expansion, zirconia partially stabilized with yttria (YSZ) is frequently employed as a ceramic topcoat of TBCs [26]. However, compared to traditional YSZ coatings, advanced thermal barrier coatings, such as rare-earth oxide ceramic compounds, have demonstrated lower thermal conductivity, higher thermal stability, and higher coefficient of thermal expansion. Studies show that doping zirconia with one or more oxides, such as Sc_2O_3, Gd_2O_3, Sm_2O_3, and Nd_2O_3, improves the thermal stability of TBCs and enables their usage at high temperatures up to 1650 °C [27].

Despite the fact that several procedures for producing porous ceramic coating and their related mechanical properties have been reported, developing a porous ceramic by the SPS process is seldom discussed in the literature. In the most recent review publication, Dudina et al. [13] also emphasized the scarcity of reports relevant to the porous ceramic produced by the SPS. Researchers found that the SPS technique densifies the material at low temperatures with shorter dwell periods than the conventional sintering process, producing material with uniform microstructure and superior mechanical characteristics [28]. Additionally, the majority of research on TBC has employed YSZ as the coating material because there are not many materials that can match the requirements for becoming TBC. Besides, they used the APS process to develop the typical YSZ TBC owing to its high deposition efficiency and low cost [29]. However, the YSZ TBCs that have undergone APS processing typically contain pores, inter-splats gaps, and microcracks that allow molten deposits to enter coatings which severely affects the mechanical and thermal integrity of the coating material [30]. Therefore, a new material system and a novel technique to process the material could be a viable solution to develop a more robust TBC system. However, very few studies have focused on alternative materials for TBCs, especially materials like Scandia stabilize Zirconia (ScSZ), which has not been extensively tested for this particular usage. Therefore, in this study, Scandia stabilized zirconia (ScSZ) materials have been chosen as a potential replacement for the conventional ceramic materials employed as TBC. Three ScSZ TBC systems have been developed in this work utilizing the Spark plasma sintering (SPS) process with varying SPS parameters to produce varied volumes of porosity. Their microstructure and mechanical characteristics have also been studied. Since the volume of porosity affects the thermo-mechanical behaviour of TBC, the mechanical properties of the materials have been defined as a function of porosity. The results are also compared with the previously developed typical YSZ system by using the atmospheric plasma spray (APS) technique.

2. Materials and methods

In this study, synthesized 8 mol% Scandia-stabilized zirconia (8-ScSZ) (Purity 99.7%) micro powder and commercially available 10 mol% Scandia-stabilized zirconia (ScSZ) (Purity 99.2%) nanopowder (purchased from Sigma Aldrich) were used as raw materials. The 8 mol% ScSZ powder was synthesized by the sol-gel process. Both the powders were mixed together to form a composite powder. The powders were mixed with a 1:1 ratio in a ball mill for 1 h to obtain homogeneous mixing. In the remaining part of the manuscript, the 10 mol% ScSZ, 8 mol% ScSZ, and composite ScSZ are referred to as 10-ScSZ, 8-ScSZ, and 10-8-ScSZ, respectively. Both the ScSZ powders and the mixed composite powder were sintered using SPS.

The fabrication of the materials was performed using a Dr Sinter Sumitomo 1050 apparatus with varying SPS parameters for instance temperature (varies from 1000 to 1200 °C), pressure (30 MPa and 60 MPa) and pressure holding time (varies from 3 to 10 min) for obtaining different porosity level. Pre-weighed powders were placed in a graphite die with a graphite foil lining. The pressure on the samples was introduced prior to the heating cycle. After that, the samples were cooled inside the furnace. The heating was performed at a rate of 100 °C/min while the cooling rate of 25 °C/min was maintained throughout the process. Finally, cylindrical pallets with 20 mm diameter and 3 mm thickness were obtained. The flow diagram of the material fabrication process is shown in Fig. 1. All the sintered samples were then polished with different grades of abrasive papers and diamond suspension to obtain mirror-polish. The samples were then cleaned with acetone and prepared for subsequent testing. Water intrusion was used to measure the porosity of the samples. The morphological analysis of the powders before and after SPS was examined by X-ray diffraction (XRD) and field-emission scanning electron microscopy (FE-SEM). The grain size was determined by using Image J software. To evaluate the grain size, the mean value of twenty (20) measurements on each sample was considered.

The micro-indentation tests were performed on the polished surface of the samples with different porosity levels using a Vickers hardness tester (Wilson Hardness: Model 402 MVD). A load of 3 N was applied for 10s to all the samples. Ten repeated measurements were performed on each pallet and the mean value was considered as the Vickers hardness (HV) value. Moreover, a conventional three-point bending test was conducted to determine the flexural strength according to ASTM C-1161-18. The tests were performed using a universal testing machine (Instron MTS 3380) with a 5 kN load cell. The pallet samples were cut into a cuboid-shaped sample with dimensions of 20 mm × 5mm × 3 mm. Three tests for each type of sample were conducted and the flexural strength was calculated. Besides, the elastic modulus (E) of the samples with different porosity was evaluated by impulse excitation technique in accordance with the guidelines of ASTM E1876. The sample was put on top of two nylon strings and then the impulse was provided on the sample by a hammer. A microphone was used to detect the acoustic signal. Finally, Poisson's ratio, as well as elastic modulus was calculated.
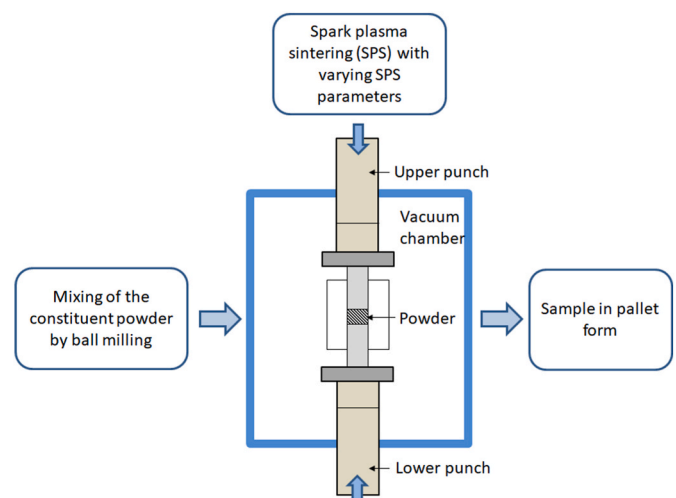

Fig. 1. Flow diagram of the material fabrication process.

3. Results and discussion

3.1. Morphology analysis

The X-ray diffraction spectra of 10-ScSZ and 8-ScSZ powders before and after sintering are shown in Fig. 2. A large peak of the tetragonal phase is observed in both the powder samples before sintering while a small peak of the monoclinic phase is noticed in the 10-ScSZ one (Fig. 2a). However, in the sintered sample of 10-ScSZ, the monoclinic phase is not observed (Fig. 2b). Both the powder samples show only the tetragonal phase indicating that the monoclinic phase which was observed initially in 10-ScSZ is fully dissolved to the tetragonal phase during the sintering process. This occurred due to the high temperature and pressure during the sintering process [28]. The morphological analysis of the powders is shown in Fig. 3. The FE-SEM micrographs show that the commercial nano 10-ScSZ grains are shaped like a sphere (Fig. 3b), whereas the grains of 8-ScSZ are in the shape of polygons (Fig. 3d). Moreover, porous agglomerates of nanopowder with a mean size of 90 nm (red dotted circle in Fig. 3a) and aggregates of micro-powder with a mean size of 45 μm (red dotted circle in Fig. 3c) were observed in the 10-ScSZ and 8-ScSZ respectively.

3.2. Porosity analysis

Table 1 represents the result of the percentage of porosity at different SPS conditions while Fig. 4 illustrates the porosity rate as a function of temperature, pressure and dwell time. It can be seen from the figure that the porosity rate of all the samples decreases with the increase in temperature, pressure and dwell time. Fig. 4a depicts the result of the porosity Vs temperature at the constant pressure of 30 MPa and dwell time of 3 min. The 8-ScSZ samples demonstrate a lower porosity rate than that of the 10-ScSZ samples until the temperature of 1120 °C, however, at 1200 °C, they exhibit a lower decrease of porosity in comparison to 10-ScSZ. The 10-ScSZ possesses a high specific surface area of 10–12 m^2/g causing a significant reactivity within the particles once the temperature rises resulting in consistent drops in porosity. Additionally, the prepared 10-8-ScSZ composite has a porosity rate that is in between that of 10-ScSZ and 8-ScSZ samples. A similar trend of porosity is also observed in all the samples prepared at high pressure of 60 MPa (Fig. 4b). In this case, a significant decrease in the total porosity is observed in all the samples as compared to the samples prepared under 30 MPa pressure.

Besides, the composite sample 10-8-ScSZ shows a lower decrease in the total porosity than the constituent materials at all temperatures, indicating that the composite ceramic possesses a large number of pores. This high existence of pores in the fabricated ceramic could be the effect of "rigid inclusion" that may occur during the sintering process of the composite ceramic. This phenomenon is also supported by some previous studies which reported that the sintering impeding occurs in the composite when fine particles and large particles are mixed together and when the size ratio of the particles increases [31]. Further, the porosity rate as a function of dwell time with the constant highest temperature of 1200 °C and the pressure of 60 MPa is depicted in Fig. 4c. A slow decline of porosity is observed in all the samples up to the dwell time of 5 min. After that, the porosity of all the samples sharply decreases once the dwell time increases to 10 min. Due to the high-pressure holding time, the reactivity of the particles increases thereby decreasing the porosity. From Fig. 4a and (b), It is observed that at comparatively low temperatures, the denseness of the 8-ScSZ samples is higher in comparison to 10-ScSZ resulting in higher reactivity between particles and reduced porosity rate. On the contrary, the densification of 10-ScSZ particles increases at high temperatures due to the fine particle size resulting in high reactivity and low porosity rate. The nanoparticles of 10-ScSZ maintain a good grain arrangement and provide a greater relative contact area between particles at high temperatures, thus decreasing the porosity. This tendency of porosity change is supported by Ahmadi et al. [32].

3.3. Microstructure analysis

Fig. 5 illustrates the microstructure of the different ScSZ materials after SPS. The surface of the pallets created under the SPS conditions of 1100 °C temperature, 60 MPa pressure, and 3 min dwell time was examined for microstructure. A homogeneous structure of nanoparticles with the existence of mesopores was observed in the pallets of 10-ScSZ (Fig. 5a). The pore size of 28 nm diameter was measured on the sintered pallets of 10-ScSZ using Image J software. Besides, an arranged macroporous microstructure was observed in the 8-ScSZ pallets (Fig. 5b). These macropores formed between the aggregates of the particles. The mean size of the grain was found to be 17 μm on the sintered 8-ScSZ pallets prepared with the same condition as mentioned above. This microstructural orientation of the grain is almost the same as the one obtained in the APS method [33]. In APS, an arranged microstructure of grain is usually obtained due to the dispersal of melted particles on the substrate surface and the cohesion of the particles depends on the contact ratio of splat. Therefore, the microstructural homogeneity in APS is highly affected by the existence of a semi-molten area in the substrate [34]. In 8-ScSZ during SPS, the cohesion of the particles depends on their shape and the densification occurs between agglomerates once the temperature and pressure reached the desired level of reactivity, thus no molten area is observed in the samples. Therefore, a better homogeneity of the microstructure is obtained in the 8-ScSZ pallets prepared by SPS in comparison to the traditional ceramic-like Yttria Stabilized Zirconia (YSZ) pallet made using the APS approach. Moreover, a homogeneous microstructure containing both mesopores and micropores can be seen in 10-8-ScSZ composite pallets (Fig. 5c). The nanoparticles of 10-ScSZ cover the porosity formed in the composite and link the 8-ScSZ aggregates (Fig. 5c).
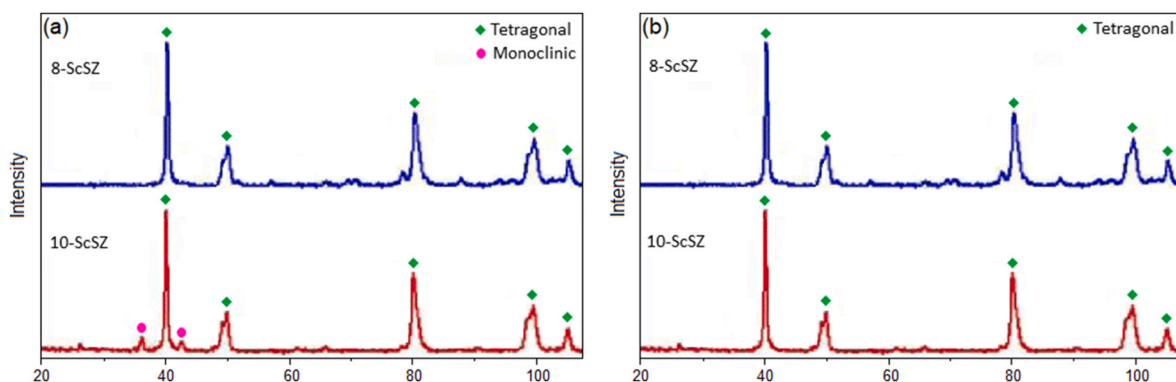

Fig. 2. X-ray diffraction spectra of 10-ScSZ and 8-ScSZ powders (a) before sintering and (b) after sintering.
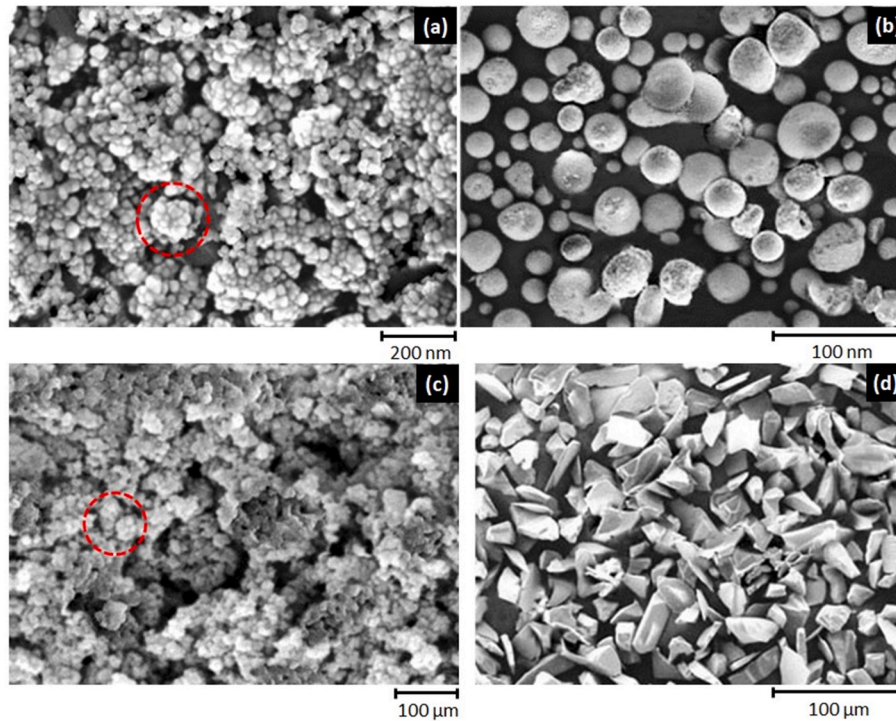
Fig. 3. FE-SEM micrograph of ScSZ powders (a) (b) 10-ScSZ powder (c) (d) 8-ScSZ powder.

Table-1
of porosity at ScSZ materials in various SPS conditions.

Constant Pressure 30 MPa, Dwell time 3 min			
Temperature (°C)	% of porosity		
	10-ScSZ	8-ScSZ	10-8-ScSZ
1000	51.8	39.6	46.1
1050	45.6	36.2	39.4
1100	37.6	33.7	33.8
1150	22.1	25.8	31
1200	11.1	17.7	20
Constant Pressure 60 MPa, Dwell time 3 min			
Temperature (°C)	% of porosity		
	10-ScSZ	8-ScSZ	10-8-ScSZ
1000	40.2	37.2	48.3
1050	34.8	33.1	37.1
1100	22.7	23.4	25.6
1150	11	17.7	22.3
1200	8.5	14.2	20.4
Constant Pressure 60 MPa and constant temperature 1200 °C			
Dwell time (Minutes)	% of porosity		
	10-ScSZ	8-ScSZ	10-8-ScSZ
3	8.5	14.2	20.4
5	7.4	13.6	19.5
10	0.6	2.3	5.7

3.4. Mechanical properties

Fig. 6 displays the result of the mechanical properties including microhardness, flexural strength and the elastic modulus of the prepared ScSZ systems as a function of porosity. The Vickers microhardness plot as shown in Fig. 6a demonstrates a decreasing trend of hardness value with the increase of porosity rate in all the samples. The 10-ScSZ exhibits a higher hardness value in comparison to other materials for all the porosity rates. This is attributed to the existence of nanopores in the material and the development of a greater contact surface between the nanoparticles. Moreover, the flexural strength was calculated as a function of the porosity rate and is illustrated in Fig. 6 (b). In this instance, the 10-ScSZ exhibits greater strength than other materials at all levels of porosity. This is also attributed to the geometry of the nanopores and larger particle contact surface [35]. Besides, according to the previous study, the cohesion strength between particles increases with the increase in their coordination number [36]. Most of the nanoparticle in 10-ScSZ are spherical in shape and possesses high coordination number resulting in high strength. Furthermore, an intermediate strength of the 10-8-ScSZ composite was observed as depicted in Fig. 6 (b). The nanoparticles of 10-ScSZ filled the gap of micropores present in the composite and increased its strength to a considerable level. In addition, the young's moduli of all the prepared pallets were calculated and the results are presented in Fig. 6c as a function of porosity. All three materials show a decrease in Young's modulus with the increase in porosity rate. The maximum values of the modulus were calculated to be 187 GPa, 160 GPa and 130 GPa for 10-ScSZ, 8-ScSZ and 10-8-ScSZ respectively. The 10-ScSZ and 8-ScSZ demonstrate a similar decreasing trend of the elastic modulus until 25% of porosity, after that, the modulus of 8-ScSZ reduces more than that of the other two materials as the porosity rate increases. However, the influence of the pore shape is not significantly noticed as was explained in the previous studies [37, 38]. At the high porosity rate, the strength of cohesion between the aggregates of 8-ScSZ reduces, thus decreasing the value of modulus sharply. The 10-8-ScSZ composite demonstrates an inferior modulus value than the two constituent materials until a 23% porosity rate and shows a greater modulus value than 8-ScSZ pallets at a high porosity rate. The lower modulus is attributed to a weak contact of 8-ScSZ aggregates and the links are only created by the 10-ScSZ nanoparticles. To compare the result, the elastic modulus of a conventional APS thermal barrier coating containing 10–20% porosity has been evaluated as a reference. The modulus of the APS material was calculated to be 22 GPa which is quite less than the modulus observed in different materials systems of ScSZ developed in SPS in this study. Previous studies explained that due to the low bonding ratio, APS materials demonstrate low modulus value which degrades the material's properties further during thermal ageing at high temperatures [34]. Therefore, it can be concluded that the ScSZ system produced by SPS can be a potential alternative to the standard YSZ coating made by the traditional APS
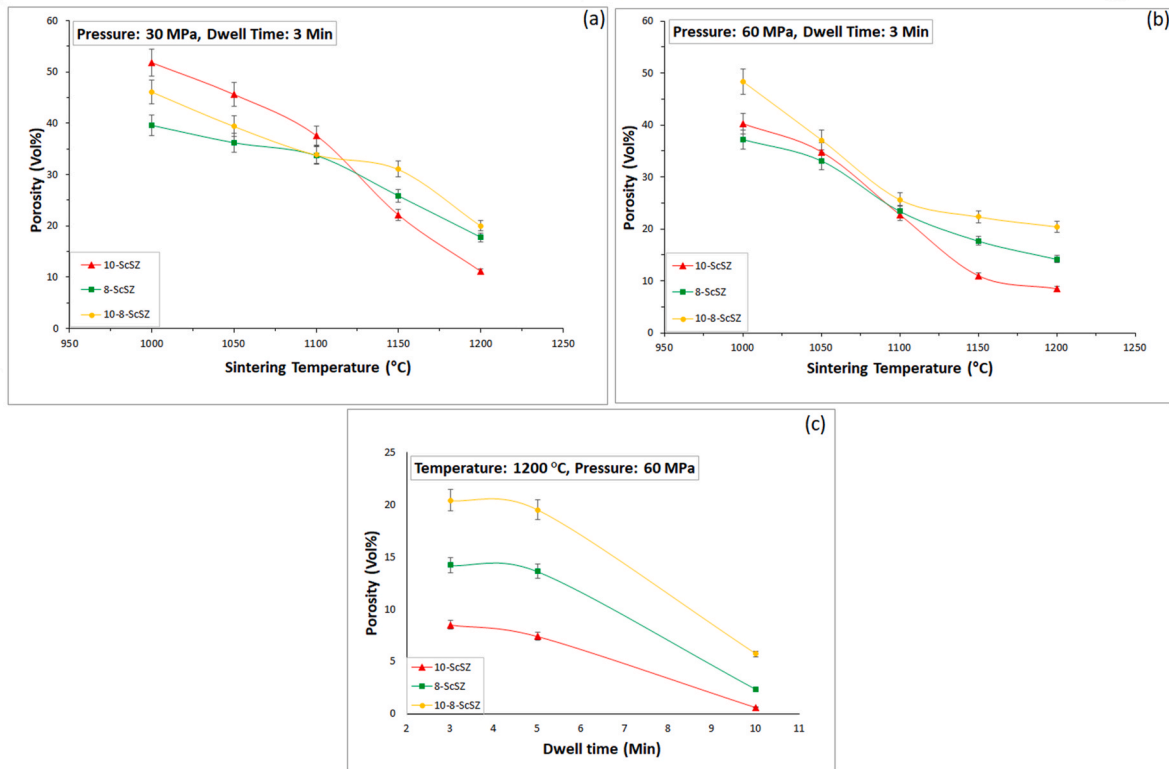
Fig. 4. Porosity of different ScSZ powders (a) porosity Vs sintering temperature (pressure 30 MPa, Dwell time 3 min), (b) porosity Vs sintering temperature (pressure 60 MPa, Dwell time 3 min), (c) porosity Vs dwell time (temperature 1200 °C, pressure 60 MPa).
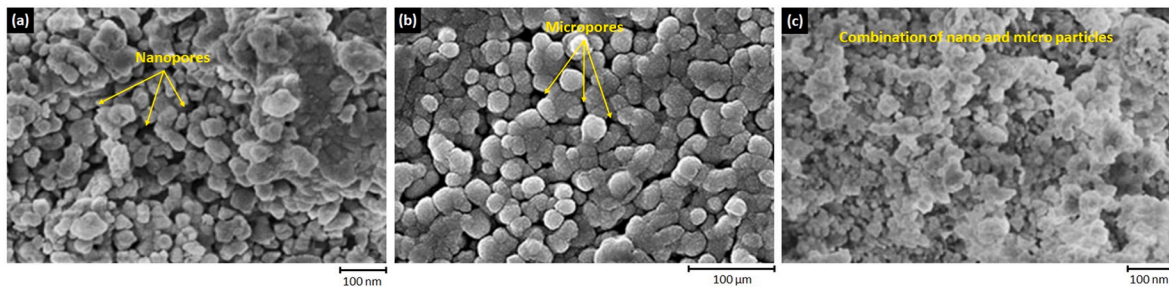

Fig. 5. Microstructure of different ScSZ systems after SPS process (a) 10-ScSZ, (b) 8-ScSZ and (c) 10-8-ScSZ (SPS condition: temperature 1100 °C, pressure 60 MPa and dwell time 3 min).

approach.

4. Conclusions

In this research, different porous scandia stabilized zirconia (ScSZ) systems have been developed by the Spark plasma sintering (SPS) process and the effect of porosity on the microstructure and mechanical properties such as hardness, strength and stiffness have been investigated. The following conclusions are obtained from the study.

i) The porosity rate of all three types of ScSZ systems decreases with increasing temperature, pressure and dwell time.
ii) At low temperatures, the micrometric 8-ScSZ shows relatively higher reactivity and lower porosity in comparison to 10-ScSZ while the nanometric 10-ScSZ illustrates better reactivity and denseness at high temperatures due to their better grain arrangement and enhancement of contact area between particles.

iii) A relatively higher porosity was observed in the 10-8-ScSZ composite in comparison to the constituent materials due to the effect of "rigid inclusion" that occurred during the SPS process.
iv) The mechanical properties such as Vickers microhardness, flexural strength and elastic modulus decrease as the porosity increase in all three types of ScSZ. Among these three materials, the nanometric 10-ScSZ demonstrates higher mechanical properties than the other two materials attributed to the presence of nanopores in the material which helps to develop a greater contact surface between the nanoparticles.
v) The SPS fabricated samples show a much higher elastic modulus value than that of the conventional APS fabricated samples while comparing the mechanical properties between the samples fabricated by two different methods.

Therefore, the porous ScSZ system developed by the SPS process could be a potential alternative thermal barrier coating (TBC) to the typical YSZ coating made by the APS technique (Table 2).
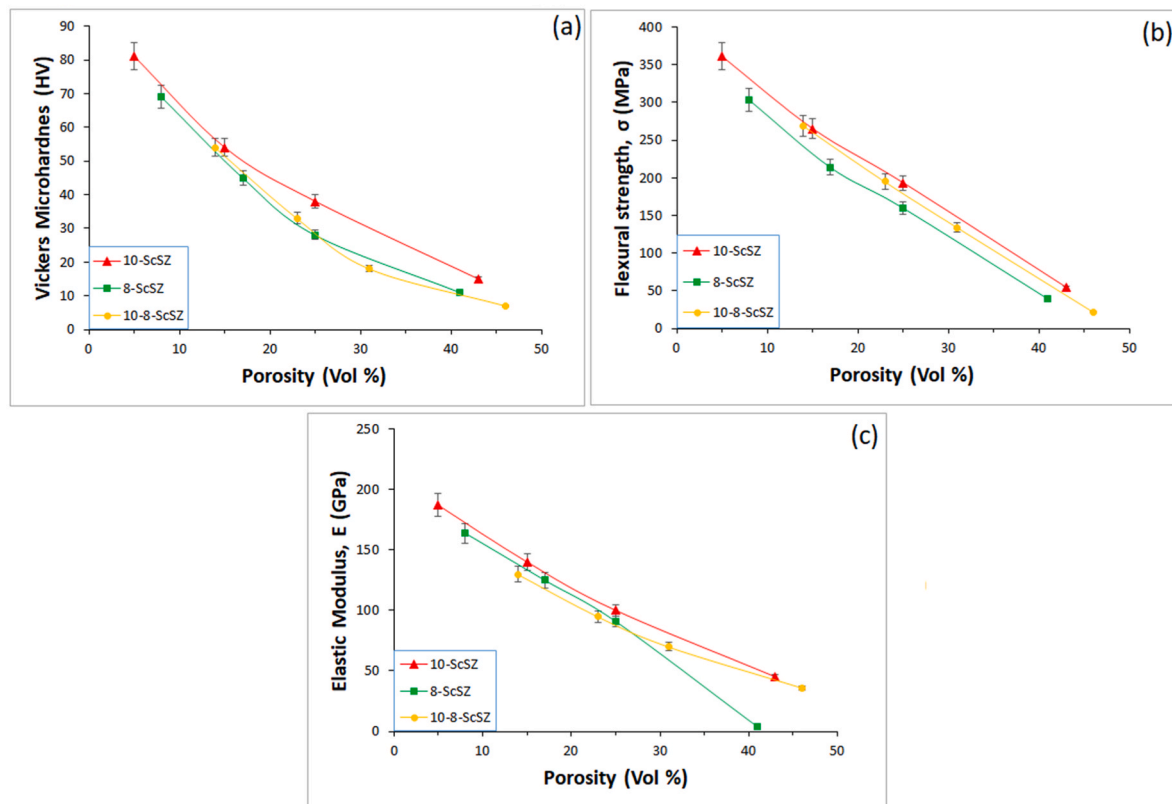
Fig. 6. Mechanical properties of different ScSZ systems as a function of porosity (a) Vickers microhardness, (b) Flexural strength and (c) Elastic modulus.

Table 2
Nomenclature.

ScSZ	Scandia stabilized zirconia
YSZ	Yittria stabilized zirconia
TBC	Thermal Barrier coating
SPS	Spark plasma sintering
APS	Atmospheric plasma spray
Sc2O3	Scandium oxide
Gd2O3	Gadolinium oxide
Nd2O3	Neodymium oxide
Sm2O3	Samarium oxide

Declaration of competing interest

The authors declare that they have no known competing financial interests or personal relationships that could have appeared to influence the work reported in this paper

Data availability

Data will be made available on request.

Acknowledgement

References

[1] M.R. Loghman-Estarki, R. Shoja, H. Edris, M. Pourbafrany, H. Jamali, R. Ghasemi, Life time of new SYSZ thermal barrier coatings produced by plasma spraying method under thermal shock test and high temperature treatment, Ceram. Int. 40 (2014) 1405–1414.

[2] X.Q. Cao, R. Vassen, D. Stoever, Ceramic materials for thermal barrier coatings, J. Eur. Ceram. Soc. 24 (2004) 1–10.

[3] M. Mrdak, M. Rakin, B. Medjo, N. Bajić, Experimental study of insulating properties and behaviour of thermal barrier coating systems in thermo cyclic conditions, Mater. Des. 67 (2015) 337–343.

[4] D.D. Hass, A.J. Slifka, H.N.G. Wadley, Low thermal conductivity vapor deposited zirconia microstructures, Acta Mater. 49 (2001) 973–983.

[5] F. Cernuschi, P. Bison, D.E. Mack, M. Merlini, S. Boldrini, S. Marchionna, S. Capelli, S. Concari, A. Famengo, A. Moscatelli, W. Stamm, Thermo-physical properties of as deposited and aged thermal barrier coatings (TBC) for gas turbines: state-of-the art and advanced TBCs, J. Eur. Ceram. Soc. 38 (2018) 3945–3961.

[6] M.P. Schmitt, J.M. Schreiber, A.K. Rai, T.J. Eden, D.E. Wolfe, Development and optimization of tailored composite TBC design architectures for improved erosion durability, J. Therm. Spray Technol. 26 (2017) 1062–1075.

[7] R. Kumar, E. Jordan, M. Gell, J. Roth, C. Jiang, J. Wang, S. Rommel, CMAS behavior of yttrium aluminum garnet (YAG) and yttria-stabilized zirconia (YSZ) thermal barrier coatings, Surf. Coat. Technol. 327 (2017) 126–138.

[8] F. Cernuschi, I.G. Golosnoy, P. Bison, A. Moscatelli, R. Vassen, H.P. Bossmann, S. Capelli, Microstructural characterization of porous thermal barrier coatings by IR gas porosimetry and sintering forecasts, Acta Mater. 61 (2013) 248–262.

[9] D.N. Boccaccini, H.L. Frandsen, S. Soprani, M. Cannio, T. Klemensø, V. Gil, P. V. Hendriksen, Influence of porosity on mechanical properties of tetragonal stabilized zirconia, J. Eur. Ceram. Soc. 38 (2018) 1720–1735.

[10] A. Afzal, M.E.M. Soudagar, A. Belhocine, M. Kareemullah, N. Hossain, S. Alshahrani, C.A. Saleel, R. Subbiah, F. Qureshi, M.A. Mujtaba, Thermal performance of compression ignition engine using high content biodiesels: a comparative study with diesel fuel, Sustainability 13 (2021) 7688.

[11] M. Reza, A. Karim, K.A. Shahab, L. Jafar, Failure analysis of overdrive gear of passenger car gearbox fabricated from powder metallurgy, Eng. Fail. Anal. 141 (2022), 106683.

[12] A.N. Keivan, N. Alireza, H. Tim, Mechanical properties and microstructure of powder metallurgy Ti-xNb-yMo alloys for implant materials, Mater. Des. 88 (2015) 1164–1174.

[13] D.V. Dudina, B.B. Bokhonov, E.A. Olevsky, Fabrication of porous materials by spark plasma sintering: a review, Materials 12 (2019) 541.

[14] E.A. Olevsky, D.V. Dudina, in: Field-Assisted Sintering: Science and Applications, Springer International Publishing, Berlin, Germany, 2018, pp. 237–274.

[15] Z.A. Munir, D. Quach, M. Ohyanagi, Electric current activation of sintering: a review of the pulsed electric current sintering process, J. Am. Ceram. Soc. 94 (2011) 1–19.

[16] C.E. Wen, M. Mabuchi, Y. Yamada, K. Shimojima, Y. Chino, H. Hosokawa, T. Asahina, Processing of fine-grained aluminum foam by spark plasma sintering, J. Mater. Sci. Lett. 22 (2003) 1407–1409.

[17] B.B. Bokhonov, D.V. Dudina, Preparation of porous materials by spark plasma sintering: peculiarities of alloy formation during consolidation of Fe@Pt core–shell and hollow Pt(Fe) particles, J. Alloys Compd. 707 (2017) 233–237.

[18] G.V. Trusov, A.B. Tarasov, D.O. Moskovskikh, A.S. Rogachev, A.S. Mukasyan, High porous cellular materials by spray solution combustion synthesis and spark plasma sintering, J. Alloys Compd. 779 (2019) 557–565.

[19] W. Pabst, Gregorova′E, G. Ticha′, Elasticity of porous ceramics-a critical study of modulus-porosity relations, J. Eur. Ceram. Soc. 26 (2006) 1085–1097.

[20] U. Anselmi-Tamburini, J.E. Garay, Z.A. Munir, A. Tacca, F. Maglia, G. Spinolo, Spark plasma sintering and characterization of bulk nanostructured fully stabilized zirconia: Part I. Densification studies, J. Mater. Res. 19 (2004) 3255–3262.

[21] G. Bernard-Granger, C. Guizard, Spark plasma sintering of a commercially available granulated zirconia powder: I. Sintering path and hypotheses about the mechanism (s) controlling densification, Acta Mater. 55 (2007) 3493–3504.

[22] W. Teguh, B.D. Djarot, S.I. Yudy, G. Femiana, Comparative microstructure characteristics and properties of arc-sprayed Fe-based and HVOF-sprayed Ni-based coatings on ASME SA 210 C steel tube, Results Eng. 17 (2023), 100985.

[23] J. Chevalier, L. Gremillard, A.V. Virkar, R.C. David, The tetragonal-monoclinic transformation in zirconia: lessons learned and future trends, Am. Sociol. 92 (2009) 1901–1920.

[24] D. Monceau, D. Oquab, C. Estournès, M. Boidot, S. Selezneff, N. Ratel-Ramond, Thermal barrier systems and multi-layered coatings fabricated by spark plasma sintering for the protection of Ni-base superalloys, Mater. Sci. Forum 654 (2010) 1826–1831.

[25] R.M. Spriggs, Expression for effect of porosity on elastic modulus of polycrystalline refractory materials, particularly aluminum oxide, J. Am. Ceram. Soc. 44 (1961) 628–629.

[26] M. Guven Gok, G. Goller, Production and characterisation of GZ/CYSZ alternative thermal barrier coatings with multi-layered and functionally graded designs, J. Eur. Ceram. Soc. 36 (2016) 1755–1764.

[27] R. Vaßen, M.O. Jarligo, T. Steinke, D.E. Mack, D. Stöver, Overview on advanced thermal barrier coatings, Surf. Coat. Technol. 205 (2010) 938.

[28] J. Chai, Y. Zhu, Z. Wang, T. Shen, Y. Liu, L. Niu, S. Li, C. Yao, M. Cui, C. Liu, Microstructure and mechanical properties of SPS sintered Al_2O_3-ZrO_2 (3Y)- SiC ceramic composites, Mater. Sci. Eng. A 781 (2020), 139197.

[29] X. Chen, Y. Zhao, X. Fan, Y. Liu, B. Zou, Y. Wang, H. Ma, X. Cao, Thermal cycling failure of new LaMgAl11O19/YSZ double ceramic top coat thermal barrier coating systems, Surf. Coating. Technol. 205 (2005) 3293–3300.

[30] M.H. Habibi, S. Yang, S.M. Guo, Phase stability and hot corrosion behavior of ZrO2–Ta2O5 compound in Na2SO4–V2O5 mixtures at elevated temperatures, Ceram. Int. 40 (2014) 4077–4083.

[31] M. Eberstein, S. Reinsch, R. Müller, J. Deubener, W.A. Schiller, Sintering of glass matrix composites with small rigid inclusions, J. Eur. Ceram. Soc. 29 (2009) 2469–2479.

[32] Z. Ahmadi, B. Nayebi, M. Shahedi, I. Farahbakhsh, Z. Balak, Densification improvement of spark plasma sintered TiB_2-based composites with micron-, submicron- and nano-sized SiC particulates, Ceram. Int. 44 (2018) 11431–11437.

[33] H.R. Abedi, M. Salehi, A. Shafyei, Mechanical and thermal properties of double-layer and triple-layer thermal barrier coatings with different ceramic top coats onto polyimide matrix composite, Ceram. Int. 43 (2017) 12770–12780.

[34] L. Wang, Y. Wang, S.G. Sun, J.Q. He, Z.Y. Pan, C.H. Wang, Microstructure and indentation mechanical properties of plasma sprayed nano-bimodal and conventional ZrO_2-8wt%Y_2O_3 thermal barrier coatings, Vacuum 86 (2012) 1174–1185.

[35] Z. Zuoguang, W. Mingchao, L. Min, Sintering and mechanical properties of mullite-reinforced boron carbide matrix composite, J. Am. Ceram. Soc. 92 (2010) 1129–1132.

[36] K. Wang, M. Zhao, X. Ren, W. Pan, High temperature mechanical properties of zirconia metastable t'-Phase degraded yttria stabilized zirconia, Ceram. Int. 45 (2019) 17376–17381.

[37] X. Fan, E.D. Case, Q. Yang, J.D. Nicholas, Room temperature elastic properties of gadolinia-doped ceria as a function of porosity, Ceram. Int. 39 (2013) 6877–6886.

[38] W. Pabst, T. Uhlířová, E. Gregorová, A. Wiegmann, Young's modulus and thermal conductivity of model materials with convex or concave pores - from analytical predictions to numerical results, J. Eur. Ceram. Soc. 38 (2018) 2694–2707.